

Fusion Complexity Inversion: Why Simpler Cross View Modules Outperform SSMs and Cross View Attention Transformers for Pasture Biomass Regression

Mridankan Mandal
Department of Information Technology
Indian Institute of Information Technology, Allahabad
Prayagraj, India
mridankanmandal2006@gmail.com

Abstract—Accurate estimation of pasture biomass from agricultural imagery is critical for sustainable livestock management, yet existing methods are limited by the small, imbalanced, and sparsely annotated datasets typical of real-world monitoring. In this study, adaptation of vision foundation models to agricultural regression is systematically evaluated on the CSIRO Pasture Biomass benchmark, a 357 image dual view dataset with laboratory validated, component wise ground truth for five biomass targets, through 17 configurations spanning four backbones (EfficientNet-B3 to DINOv3-ViT-L), five cross view fusion mechanisms, and a 4×2 metadata factorial. A counterintuitive principle, termed *fusion complexity inversion*, is uncovered: on scarce agricultural data, a two layer gated depthwise convolution ($R^2=0.903$) outperforms cross view attention transformers (0.833), bidirectional SSMs (0.819), and full Mamba (0.793, below the no-fusion baseline). Backbone pretraining scale is found to monotonically dominate all architectural choices, with the DINOv2→DINOv3 upgrade alone yielding $+5.0 R^2$ points. Training only metadata (species, state, and NDVI) is shown to create a universal ceiling at $R^2 \approx 0.829$, collapsing an 8.4 point fusion spread to 0.1 points. Actionable guidelines for sparse agricultural benchmarks are established: backbone quality should be prioritized over fusion complexity, local modules preferred over global alternatives, and features unavailable at inference excluded.

Keywords: pasture biomass estimation, foundation models, agricultural imagery, dual view fusion, sparse annotations, precision agriculture.

I. INTRODUCTION

Scalable, non-destructive estimation of crop and pasture properties from imagery alone is increasingly enabled by computer vision [20]. Pasture biomass estimation, the prediction of dry matter weight of vegetation components from field photographs, is a canonical agricultural vision task requiring fine grained pattern recognition, robustness to sparse and imbalanced annotations, and generalization across geographic and seasonal conditions. Traditional methods (like rising plate meters, and destructive harvesting) cannot scale to the millions of hectares under pastoral management, motivating vision based alternatives.

Self supervised vision transformers pretrained at scale, notably DINOv2 [17] and DINOv3 [18] (up to 1.7B images),

now provide general purpose encoders that transfer to narrow agricultural domains with minimal task specific data [28], [4]. Scale dependent transfer has been further demonstrated by vision language [27] and large language models [29]. A critical question remains, however: Given a powerful pretrained backbone, how much task specific complexity should be added when training data is scarce?

The CSIRO Pasture Biomass dataset [15], the first publicly available, multi-site pasture resource combining visual, spectral, and structural modalities with laboratory validated, component wise ground truth, is adopted as the benchmark. Unlike prior datasets relying on visual estimation or single site collection, CSIRO spans 19 sites across four Australian states over three years (2014–2017), with consumer grade cameras under natural lighting. Each of 357 dual view training photographs is paired with destructive cut-dry-weigh measurements: vegetation within a $70 \text{ cm} \times 30 \text{ cm}$ quadrat is harvested, sorted into green, dead, and clover fractions, oven dried at 70°C for 48h, and laboratory weighed, producing ground truth unmatched by any comparable benchmark. Three targets show significant zero inflation (up to 37.8% for clover), and right skewed distributions. Auxiliary metadata (species, state, NDVI, height, and date), available only during training, creates a realistic modality shift scenario common in agricultural deployment.

A systematic study spanning 17 configurations is presented along three axes: (1) cross view fusion complexity (identity, gated depthwise convolution, cross-view gated attention transformer, bidirectional Mamba SSM, and full Mamba SSM), (2) backbone scale (EfficientNet-B3 [30] through DINOv3-ViT-L, spanning ImageNet-1K [39] to LVD-1.7B), and (3) training only metadata fusion. All experiments are conducted with identical recipes, 5 fold stratified group cross validation, and a single 8 GB consumer GPU.

Three principal findings are established. (1) **Fusion complexity inversion:** a two layer gated depthwise convolution ($R^2=0.903$) outperforms all global alternatives, and full Mamba (0.793) falls below the no fusion baseline. (2) **Found-**

Foundation model scale dominance: R^2 increases monotonically from EfficientNet-B3 (0.555) to DINOv3-ViT-L (0.903), and the DINOv2→DINOv3 upgrade alone yields +5.0 points. (3) **Metadata fusion can harm:** training only metadata collapses all fusion types to $R^2 \approx 0.829$, destroying the best model’s 7.4 point advantage. Feature space analysis of image derived color indices and sensor metadata reveals moderate correlations between simple hand crafted features and biomass components, establishing an interpretable baseline that learned representations must surpass.

II. RELATED WORK

Computer vision for agricultural imagery. Crop and pasture analysis has progressed from hand crafted vegetation indices [2], [9], [20] to CNN based proximal sensing [10], [19], composition classification [33], and aerial monitoring [40]. A persistent bottleneck in agricultural vision is the scarcity of annotated data. The CSIRO Pasture Biomass dataset [15] exemplifies this: laboratory validated, component wise ground truth (destructive cut-dry-weigh) is paired with heterogeneous inputs (imagery, NDVI, and compressed height) across 19 sites in four Australian states, yet only 357 training images are provided, with significant zero inflation and right skewed targets.

Foundation models in agriculture. Self supervised pre-training at scale has been catalyzed by the vision transformer paradigm [26], [31]. DINO [4], DINOv2 [17] (LVD-142M), and DINOv3 [18] (LVD-1.7B) learn label free features adopted for remote sensing [5] and plant phenotyping [11], and complementary signals are provided by masked autoencoders [28]. Scale dependent transfer has been confirmed by vision language [27] and large language models [29], yet systematic guidance on task specific complexity atop foundation models for scarce agricultural data is lacking. This gap is addressed here by quantifying backbone–fusion interactions on a small agricultural benchmark.

Efficient training on sparse agricultural data. Differential learning rates [13], gradient checkpointing, mixed precision training [14], data augmentation [30], [38], and robust loss functions [36] enable fine tuning of large backbones on consumer hardware. In this study, $R^2=0.903$ is achieved on 357 images without external data through these strategies combined with an appropriate foundation model.

Data fusion and auxiliary metadata integration. Dual branch architectures employ cross attention [21], [22], concatenation [3], [6], or late fusion [7], and ModDrop [41] provides robustness to missing modalities. Metadata fusion is common in remote sensing [1], [8], and Gaussian process regression [34] provides a probabilistic framework for sparse data regression. Selective SSMs (Mamba [12]) have been adapted for vision through VMamba [16], with bidirectional [23], [24] and hybrid [25] variants. Five fusion paradigms are benchmarked here, and local fusion is found to dominate all global alternatives. Training only metadata is shown to act as a harmful shortcut ($-7.4 R^2$ points).

III. METHOD

A. Problem Formulation

Given a dual view pasture photograph, the task is to predict five biomass targets: Dry Green (g), Dry Dead (g), Dry Clover (g), Green Dry Matter (GDM = Green + Clover), and Dry Total (Total = GDM + Dead). All targets are $\log(1+y)$ transformed to stabilize variance across right skewed distributions. The primary metric is a weighted R^2 :

$$R^2_{\text{weighted}} = \sum_{i=1}^5 w_i \cdot R_i^2, \quad w = [0.1, 0.1, 0.1, 0.2, 0.5] \quad (1)$$

where the weights reflect agronomic priorities: Dry Total (50%) is the primary indicator of carrying capacity, GDM (20%) measures digestible fraction, and the three components each receive 10%.

B. Dual View Input Pipeline

Each input image ($\sim 2000 \times 1000$ pixels) captures a 70 cm \times 30 cm pasture quadrat from above, split vertically into left/right halves and resized to 512×512 with area-based resampling (INTER_AREA). Both halves are normalized with ImageNet statistics and pass through a weight tied backbone, halving the parameter count relative to independent encoders while providing complementary spatial coverage of the quadrat. The resulting token sequences (1024×1024 each) are concatenated to form a 2048×1024 joint representation before fusion.

C. Architecture

The model comprises four components: a weight tied backbone, a local fusion module, adaptive pooling, and compositional prediction heads (Figure 1).

Backbone. DINOv3-ViT-L (303.08M parameters, 24 transformer layers) pretrained on LVD-1.7B is used. Each 512×512 view yields a $32 \times 32 = 1024$ token grid of dimension 1024. Gradient checkpointing fits the dual-view forward pass within 8 GB VRAM. The backbone is fine-tuned at 1×10^{-5} , while task specific layers use 5×10^{-4} .

Fusion: Gated Depthwise Convolution. The concatenated 2048×1024 token sequence is processed by two stacked GatedDepthwiseConvBlocks, combining depthwise separable convolution [38] with multiplicative gating [37]. Each block applies LayerNorm, sigmoid gating, depthwise 1D convolution ($k=5$), linear projection with dropout ($p=0.2$), and a residual connection:

$$\text{GatedDWConv}(x) = x + \text{Drop}\left(W_p \cdot \text{DWConv}_{k=5}\left(\text{LN}(x) \odot \sigma(W_g \cdot \text{LN}(x))\right)\right) \quad (2)$$

Two stacked blocks have an effective receptive field of 9 tokens. This local operation does not attend across the full sequence: the backbone’s self attention already captures global dependencies within each view. Total fusion parameters: 4.21M.

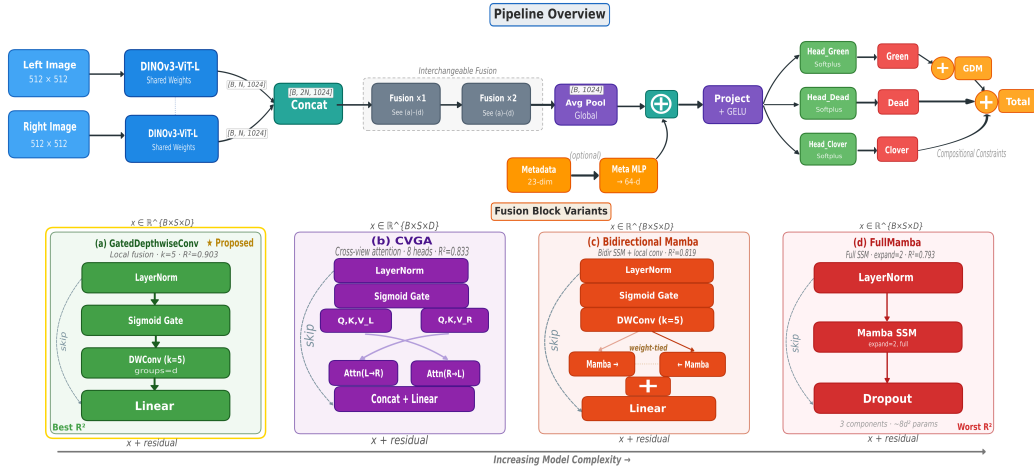


Fig. 1. Architecture overview of the proposed dual-view biomass regression pipeline. Each input image is split into left/right halves, encoded by a weight-tied DINOv3-ViT-L backbone, and fused through two stacked GatedDepthwiseConv blocks before compositional prediction heads.

Prediction Heads. Three independent heads (Green, Dead, and Clover) map the average pooled 1024-d vector to scalars through a two layer MLP with Softplus output:

$$\text{head}(x) = \text{Softplus}(W_2 \cdot \text{Drop}(\text{GELU}(W_1 \cdot x))) \quad (3)$$

Composite targets are computed by summation: $\text{GDM} = \text{Green} + \text{Clover}$, $\text{Total} = \text{GDM} + \text{Dead}$. Total task specific parameters: 5.79M (1.9% of the 308.87M total), comprising 4.21M fusion and 1.58M heads. No metadata is used at training or inference.

D. Baseline Fusion Mechanisms

Four alternative fusion modules are benchmarked with the same DINOv3-ViT-L backbone, training recipe, and cross validation protocol.

Cross View Gated Attention (CVGA). The concatenated sequence is split into left and right halves, and bidirectional cross attention (8 heads, $d_h=128$) with sigmoid gating enables global cross view interaction at $O(N^2)$ cost. Two blocks: 10.50M parameters.

Bidirectional Mamba SSM (BidirMamba). Combines local depthwise convolution ($k=5$) with weight tied bidirectional Mamba SSM ($d_{\text{state}}=16$, $\text{expand}=2$) for global $O(N)$ sequence modeling. Requires FP32 due to CUDA kernel constraints. Two blocks: 17.55M parameters.

Full Mamba SSM (MambaFusionBlock). Unidirectional Mamba with $\text{expand}=2$ and no gating or depthwise convolution overhead, making each block leaner than BidirMamba despite the same expand factor. Two blocks: 13.34M parameters.

Identity (no fusion). The concatenated sequence passes directly to pooling with no learned cross view interaction (zero parameters).

Table I summarizes all fusion blocks.

TABLE I
FUSION BLOCK COMPARISON SUMMARY.

Property	GatedDWConv	CVGA	BidirMamba	FullMamba	Identity
Receptive field	Local ($k=5$)	Global $O(N^2)$	Local+Global	Global $O(N)$	None
Params/block	2.11M	5.25M	8.77M	6.67M	0
Total (2 blocks)	4.21M	10.50M	17.55M	13.34M	0
AMP compatible	Yes	Yes	No	No	Yes

E. Metadata Injection (Ablation Variant)

For metadata inclusive experiments, the CSIRO training set’s auxiliary information is encoded into a 23 dimensional vector: State (one hot, 4d), Species (one hot, 15d), NDVI (1d), Height (1d), and cyclical sampling month (2d). A two layer MLP ($23 \rightarrow 64$, 1.12M parameters) produces a metadata embedding that is concatenated with the 1024-d pooled image features and projected back to 1024 dimensions. During training, the metadata vector is zeroed with probability $p=0.2$ per sample, and at test time, metadata is absent entirely. As shown in Section IV-F, this dropout rate is insufficient to prevent the metadata shortcut.

IV. EXPERIMENTS

A. Dataset

The competition subset of the CSIRO Pasture Biomass dataset [15] comprises 357 dual view photographs from 19 sites across four Australian states (2014–2017), selected from 3,187 samples through rigorous quality control. At each site, vegetation within a $70 \text{ cm} \times 30 \text{ cm}$ quadrat was photographed with consumer grade cameras under natural lighting, then harvested, sorted into green, dead, and clover fractions ($\geq 30 \text{ g}$ subsample), oven dried at 70°C for 48 h, and laboratory weighed. CSIRO is the first public pasture benchmark to provide separate dead matter annotations, and to combine visual, spectral (GreenSeeker NDVI, 100 reading average), and structural (falling plate meter) modalities.

TABLE II
TARGET VARIABLE STATISTICS IN THE TRAINING SET ($n = 357$).

Target	w	Mean	Std	Min	Med.	Max	Skew	Zero%
Dry Green	0.1	26.6	25.4	0.0	20.8	158.0	1.75	5.0
Dry Dead	0.1	12.0	12.4	0.0	8.0	83.8	1.76	11.2
Dry Clover	0.1	6.7	12.1	0.0	1.4	71.8	2.84	37.8
GDM	0.2	33.3	24.9	1.0	27.1	158.0	1.56	0.0
Dry Total	0.5	45.3	28.0	1.0	40.3	185.7	1.43	0.0

All five biomass targets are right skewed (skewness 1.4–2.8), with Dry Clover showing 37.8% zero values (Figure 2). The heavy right tails motivate the $\log(1+y)$ transform, and composite targets (GDM, Dry Total) have no zeros by construction. Table II provides summary statistics.

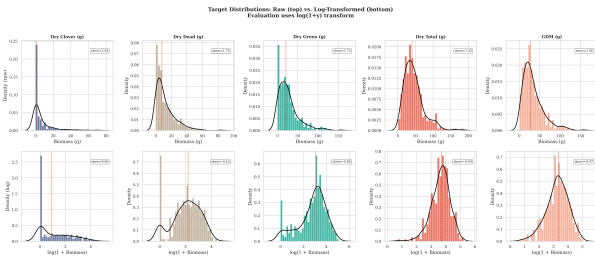


Fig. 2. Histograms of the five biomass target variables in the training set ($n = 357$).

Correlation structure. Figure 3 presents the Pearson correlation matrix among all five biomass targets and four metadata variables. Dry Green and GDM are highly correlated ($r = 0.98$) by construction, as are GDM and Dry Total ($r = 0.90$). Auxiliary metadata includes NDVI ($r=0.54$ with green biomass), compressed height ($r=0.48$ with total biomass), pasture species, state, and sampling date, all absent at test time.

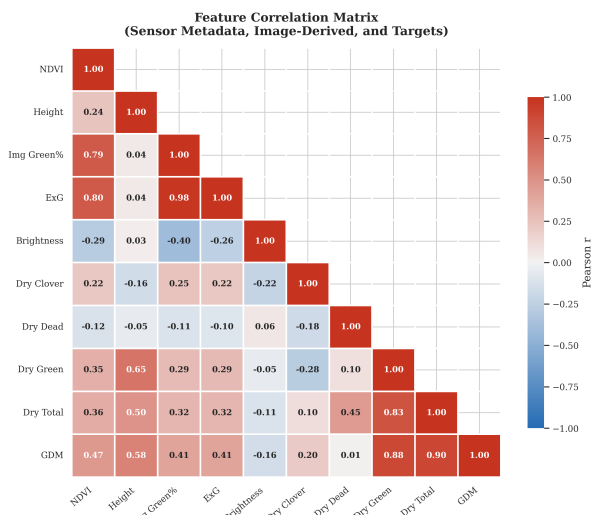


Fig. 3. Pearson correlation heatmap among biomass targets and metadata variables.

Figure 4 visualizes metadata–biomass relationships: both correlations show substantial scatter, confirming genuine but insufficient signal, and incorporating metadata degrades the best model by 7.4 R^2 points (Section IV-F).

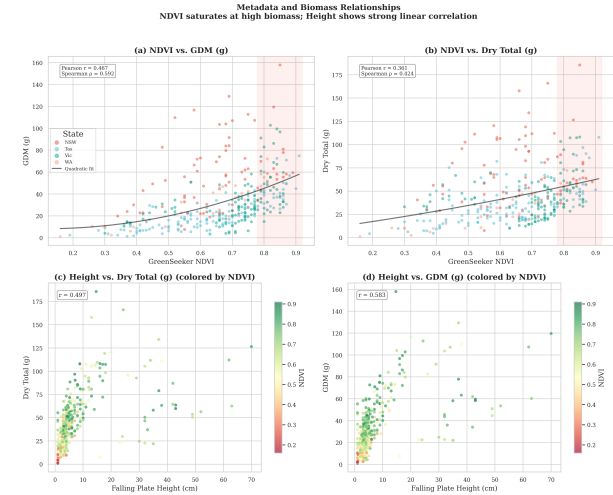


Fig. 4. NDVI and compressed height vs. biomass scatter plots, colored by pasture species.

Geographic and seasonal variation. Victoria and Tasmania show higher median biomass (~ 50 – 55 g) than NSW and WA (~ 30 – 40 g), though substantial interquartile overlap indicates state alone is a weak predictor (Figure 5). Collection peaks in spring and autumn (Figure 6), and species composition spans 15 types dominated by ryegrass-clover mixtures (Figure 7), and lucerne has higher average biomass, but wide per species ranges motivate the visual only approach.

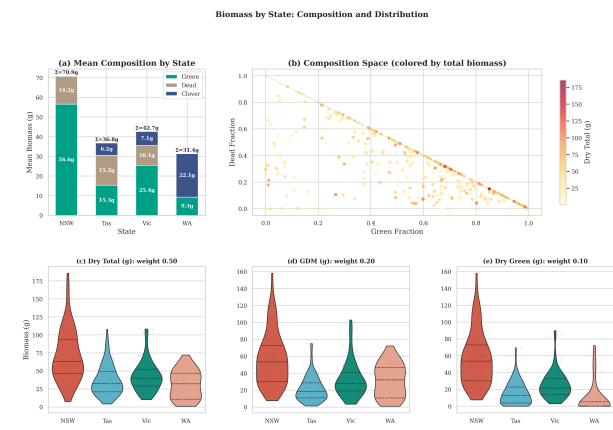


Fig. 5. Dry Total biomass distributions by Australian state.

B. Cross-Validation Protocol

All models are evaluated with 5-fold Stratified Group K-Fold cross validation (scikit-learn, and seed 17). Folds are stratified on Dry Total quintiles, and grouped by image ID to prevent leakage. Each fold contains ~ 71 validation and ~ 286 training images. Models train for up to 50 epochs with

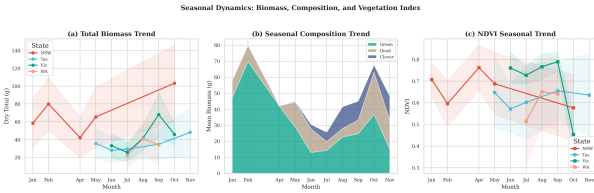


Fig. 6. Temporal distribution of sampling dates and seasonal biomass dynamics.

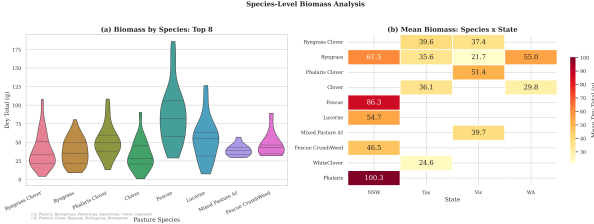


Fig. 7. Species distribution and associated biomass ranges in the training set.

early stopping (patience 10) on validation weighted R^2 . All 17 configurations converged before the 50 epoch maximum, with training halted by early stopping in every case. A single master seed controls all randomness across the 17 configurations.

C. Training Configuration

All experiments use AdamW [13] with differential learning rates (1×10^{-5} backbone, 5×10^{-4} heads), weight decay 10^{-2} , cosine annealing with 5 epoch linear warmup, Huber loss [36] ($\beta=5.0$) on $\log(1+y)$ targets, and gradient clipping at 1.0. Differential rates preserve pretrained backbone representations while accelerating randomly initialized heads. Mixed precision (FP16) is used for AMP compatible blocks (GatedDWConv, CVGA), while Mamba blocks require FP32, consuming $1.5 \times$ more VRAM. Gradient checkpointing trades $\sim 30\%$ computation for 40% VRAM reduction, essential for dual view DINOv3-ViT-L on 8 GB. Augmentations (flip, rotation $\pm 15^\circ$, shift-scale-rotate, and color jitter) are applied identically to both views through albumentations, and no test time augmentation (TTA) is used. All experiments run on a single NVIDIA RTX 4060 Laptop GPU (8 GB VRAM), with each 5 fold CV run requiring 4–8 hours.

D. Main Results

Table III presents all 17 configurations. The proposed model (DINOv3-ViT-L + $2 \times$ GatedDWConv, no metadata) achieves $R^2=0.903 \pm 0.064$, outperforming all alternatives by at least 5 points. A dense cluster of DINOv3 based models occupies the 0.81–0.85 range regardless of fusion mechanism, while VMamba based models (~ 0.72), and EfficientNet-B3 (0.555) form progressively weaker tiers. Figure 8(b) reveals a near linear relationship between log pretraining scale and downstream R^2 .

The median predictor (B1, $R^2=-0.065$) and zero shot DINOv2+ConvNeXt (B3, $R^2=-1.999$) confirm that neither constant prediction nor off the shelf features are viable, with

TABLE III
MAIN RESULTS. ALL MODELS ARE EVALUATED THROUGH 5-FOLD STRATIFIED GROUP CROSS-VALIDATION ON THE CSIRO TRAINING SET ($n = 357$). WEIGHTED R^2 ON $\log(1+y)$ TARGETS IS REPORTED. BEST IN BOLD.

ID	Model	Backbone	Fusion	Meta	$R^2 \uparrow$	Std \downarrow
B1	Median Predictor	None	None	No	-0.065	0.006
B3	DINOv2+ConvNeXt ZS	ViT-B/14	Ensemble	No	-1.999	0.341
B2	EfficientNet-B3	EffNet-B3	Single-view	No	0.555	0.084
B9	VMamba+Mamba	VMamba-B	$2 \times$ Mamba	No	0.717	0.052
B6	VMamba+Mamba	VMamba-B	$2 \times$ Mamba	Yes	0.743	0.048
E5	DINOv3+FullMamba	DINOv3-L	$2 \times$ Mamba	No	0.793	0.034
E7	DINOv3+4 \times GDWC	DINOv3-L	$4 \times$ GDWC	No	0.814	0.039
E4	DINOv3+Identity	DINOv3-L	Identity	No	0.819	0.055
E1	DINOv3+BidirMamba	DINOv3-L	$2 \times$ BidirM	No	0.819	0.051
E6	DINOv3+1 \times GDWC	DINOv3-L	$1 \times$ GDWC	No	0.821	0.034
E8	DINOv3+Identity+M	DINOv3-L	Identity	Yes	0.828	0.053
B8	DINOv3+BidirM+M	DINOv3-L	$2 \times$ BidirM	Yes	0.829	0.042
E3	DINOv3+GDWC+M	DINOv3-L	$2 \times$ GDWC	Yes	0.829	0.045
B7	DINOv3+CVGA+M	DINOv3-L	$2 \times$ CVGA	Yes	0.830	0.050
E2	DINOv3+CVGA	DINOv3-L	$2 \times$ CVGA	No	0.833	0.051
B4	DINOv2+GDWC	DINOv2-L	$2 \times$ GDWC	No	0.853	0.097
B5	DINOv3+GDWC	DINOv3-L	$2 \times$ GDWC	No	0.903	0.064

TABLE IV
FUSION COMPARISON ON DINOv3-ViT-L, NO METADATA.

Rank	Fusion	ID	$R^2 \uparrow$	Std \downarrow	Complexity
1	$2 \times$ GatedDWConv	B5	0.903	0.064	$O(Nk)$
2	$2 \times$ CVGA	E2	0.833	0.051	$O(N^2)$
3	$1 \times$ GatedDWConv	E6	0.821	0.034	$O(Nk)$
4	Identity (no fusion)	E4	0.819	0.055	$O(1)$
5	$2 \times$ BidirMamba	E1	0.819	0.051	$O(N)$
6	$4 \times$ GatedDWConv	E7	0.814	0.039	$O(Nk)$
7	$2 \times$ FullMamba	E5	0.793	0.034	$O(N)$

B3’s negative score underscoring the necessity of task specific training. Among fine tuned models, a clear three tier hierarchy emerges: DINOv3 (0.793–0.903), VMamba (0.717–0.743), and EfficientNet-B3 (0.555), aligning with pretraining data scale.

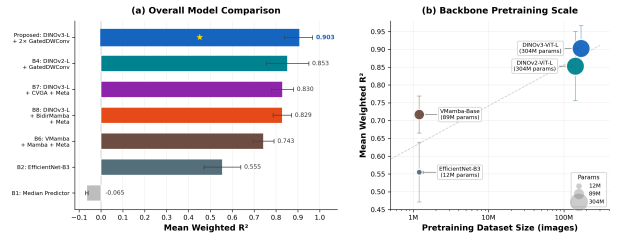


Fig. 8. Main results across all 17 configurations.

E. Fusion Complexity Analysis

Table IV isolates fusion complexity effects on DINOv3-ViT-L without metadata.

Three patterns emerge. (1) BidirMamba ($R^2=0.819$) matches the no-fusion identity baseline despite having the highest parameter count (17.55M), while FullMamba (0.793) falls 2.6 points below identity with 13.34M fusion parameters, establishing a negative correlation between fusion parameters and performance. (2) The GatedDWConv depth curve traces an inverted U: 0 blocks (0.819) \rightarrow 1 (0.821) \rightarrow 2 (**0.903**)

TABLE V
FUSION \times METADATA FACTORIAL ON DINOv3-ViT-L.

Fusion	No Meta ($R^2 \uparrow$)	With Meta ($R^2 \uparrow$)	Δ
2 \times GatedDWConv	0.903 (B5)	0.829 (E3)	-0.074
2 \times CVGA	0.833 (E2)	0.830 (B7)	-0.003
2 \times BidirMamba	0.819 (E1)	0.829 (B8)	+0.010
Identity	0.819 (E4)	0.828 (E8)	+0.009
Δ (Fusion Effect)	+0.084	+0.001	

→ 4 (0.814). The disproportionate 1-to-2 block jump (+8.2 points) suggests that the 9-token receptive field captures a critical spatial scale at the left-right boundary, while the 2-to-4 drop (-8.9) signals overfitting. (3) CVGA (0.833) outperforms both SSM variants but trails 2 \times GatedDWConv by 7.0 points: quadratic attention’s expressiveness is offset by overfitting on 286 training images per fold. Figure 9 visualizes these results.

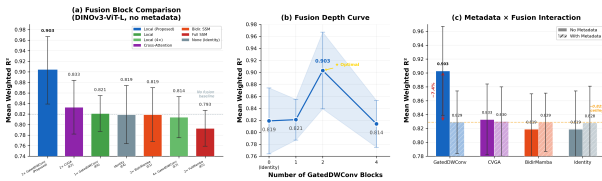


Fig. 9. Ablation studies: (a) fusion type comparison, (b) fusion depth curve, (c) metadata interaction heatmap.

F. The Metadata Paradox

Table V presents a 4 \times 2 factorial crossing fusion type with metadata on/off on DINOv3-ViT-L.

Without metadata, the fusion spread is 8.4 R^2 points, and with metadata, it collapses to 0.1 points as all configurations converge to $R^2 \approx 0.829$. Metadata *destroys* the best model: GatedDWConv drops from 0.903 to 0.829 (-7.4 points). The mechanism is straightforward: during training, species and state metadata provide predictive shortcuts through the MLP, and at test time, metadata is absent, and GatedDWConv suffers the largest degradation from this distribution shift. The Δ column reveals an asymmetry: weaker models (Identity, BidirMamba) gain slightly (+0.009 to +0.010), CVGA shows near zero effect (-0.003), and GatedDWConv is harmed most (-0.074). Metadata harm is proportional to model quality: the better the visual backbone, the more important it is to exclude training only metadata.

G. Backbone Pretraining Scale

Table VI controls for backbone scale with matched fusion and no metadata.

Performance is strictly monotonic with pretraining scale. The DINOv2→DINOv3 transition keeps architecture fixed while increasing pretraining data from 142M to 1.7B images, yielding +5.0 R^2 points with zero additional parameters. Across the full backbone range, pretraining scale contributes +34.8 points (EfficientNet-B3 to DINOv3), far exceeding the

TABLE VI
BACKBONE PRETRAINING SCALE VS. DOWNSTREAM R^2 .

Backbone	Pretrain Data	Params	$R^2 \uparrow$	$\Delta \uparrow$
EfficientNet-B3	ImageNet-1K (1.2M)	10.70M	0.555	baseline
VMamba-Base	ImageNet-1K (1.2M)	88.56M	0.717	+0.162
DINOv2-ViT-L	LVD-142M	304.37M	0.853	+0.298
DINOv3-ViT-L	LVD-1.7B	303.08M	0.903	+0.348

maximum fusion (+8.4) or metadata (± 7.4) effects. VMamba-Base (0.717), despite 8.3 \times more parameters than EfficientNet-B3, remains far below DINOv2 (-13.6), confirming that pretraining data dominates architecture choice. Practically, upgrading from DINOv2 to DINOv3 (+5.0 points, zero additional parameters, no overfitting risk) provides the most efficient single improvement, and the log-linear relationship in Figure 8(b) suggests continued data scaling would yield predictable gains.

H. Feature Space Analysis

Figure 10 examines the relationship between image derived color indices, sensor metadata, and biomass targets. The Excess Green Index (ExG) is moderately correlated with GDM ($\rho=0.525$) and Image Greenness with Dry Green ($\rho=0.404$), whereas Mean Brightness shows negligible association with Dry Dead ($\rho=0.102$), indicating that simple color features capture green biomass signals, but fail for senescent material. The NDVI \times Height hexbin plot reveals that these two sensor metadata variables jointly stratify mean Dry Total across most of its range, explaining why metadata fusion improves weaker backbones, but saturates for DINOv3, which already encodes equivalent visual cues. The state level density plot further shows that geographic provenance induces distinct clusters in the NDVI-Height space, motivating the stratified group cross validation protocol adopted in Section IV. Figure 11 shows spatial feature maps overlaid on representative images: DINOv3 produces spatially coherent activations that cleanly segment green vegetation from dead material, DINOv2 shows similar but less refined selectivity, and VMamba-Base produces coarser maps, paralleling the R^2 ranking and confirming that spatial discrimination, not fusion capacity, is the primary bottleneck.

I. Fold Analysis and Stability

Figure 12 shows per-fold R^2 for all DINOv3-based models. Fold 4 is consistently hardest across every model (5-12 point drops), suggesting edge case pasture conditions: under represented species, atypical seasonal states, and a higher proportion of low biomass clover dominant swards, rather than a model specific failure. Table VII details Fold 4 performance: the proposed model (B5) achieves the highest score (0.779), but shows the largest drop (-0.125), revealing a performance stability tradeoff.

Table VIII presents stability analysis: the proposed model’s CV of 7.0% is moderate, while the most stable models (FullMamba 4.3%, 1 \times GatedDWConv 4.2%) achieve lower

Feature Space Analysis: Image-Derived Colors and Sensor Metadata Color features are available at test time; NDVI and Height are not

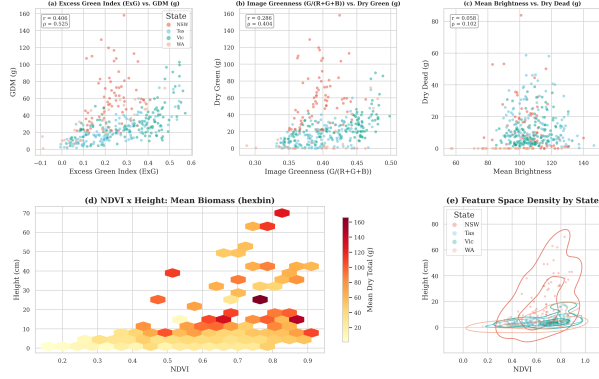


Fig. 10. Feature space analysis. (a)–(c) Image derived color indices versus biomass targets, colored by state. (d) NDVI×Height hexbin colored by mean Dry Total. (e) State level density in the NDVI–Height plane.

Backbone Feature Activation Comparison
Feature Norms: DINOv2, DINOv3, and VMamba (ImageNet Pretrained)

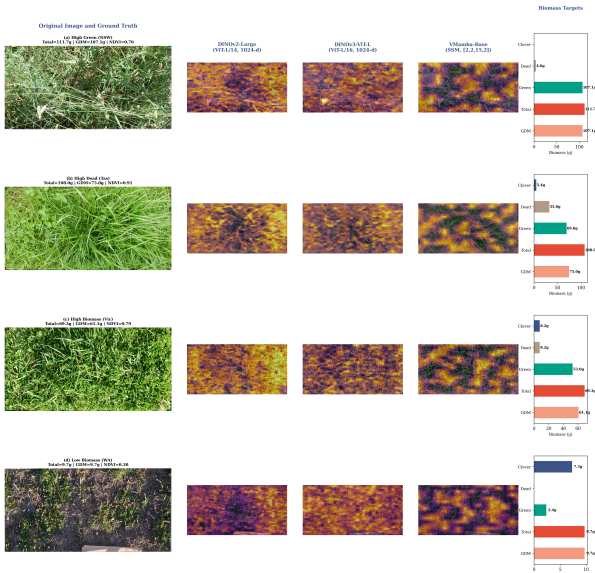


Fig. 11. Spatial feature map visualizations from three backbone architectures.

R^2 . Metadata models cluster at lower CV (5.1–6.0%) because the ceiling suppresses both peaks and troughs, and practitioners valuing consistency may prefer 1 block GatedDWConv (CV=4.2%, $R^2=0.821$).

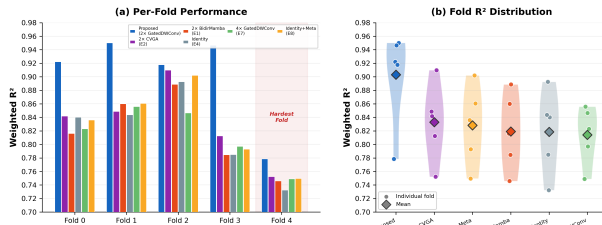


Fig. 12. Per-fold performance analysis across DINOv3-based configurations.

TABLE VII

FOLD 4 PERFORMANCE (HARDEST FOLD) FOR DINOv3-BASED CONFIGS.

Model	Fold 4 $R^2 \uparrow$	Drop \uparrow
E4: Identity	0.732	-0.086
E1: BidirMamba	0.746	-0.073
B7: CVGA+Meta	0.749	-0.081
E7: 4×GDWC	0.749	-0.065
E2: CVGA	0.752	-0.081
E3: GDWC+Meta	0.758	-0.071
B8: BidirMamba+Meta	0.761	-0.068
E6: 1×GDWC	0.761	-0.060
B5: Proposed	0.779	-0.125

TABLE VIII

STABILITY ANALYSIS (COEFFICIENT OF VARIATION, LOWER IS MORE STABLE).

Model	$R^2 \uparrow$	Std \downarrow	CV (%) \downarrow
E5: FullMamba	0.793	0.034	4.3
E6: 1×GDWC	0.821	0.034	4.2
E7: 4×GDWC	0.814	0.039	4.7
B8: BidirMamba+M	0.829	0.042	5.1
E3: GDWC+Meta	0.829	0.045	5.4
B7: CVGA+Meta	0.830	0.050	6.0
E1: BidirMamba	0.819	0.051	6.2
E2: CVGA	0.833	0.051	6.2
E4: Identity	0.819	0.055	6.7
B5: Proposed	0.903	0.064	7.0
B4: DINOv2+GDWC	0.853	0.097	11.4
B2: EffNet-B3	0.555	0.084	15.0

J. Prediction Quality Analysis

Figure 13 shows predicted vs. actual scatter plots for all five targets ($\log(1+y)$) of the proposed model (B5, $R^2=0.903$). Predictions cluster tightly around the identity line, with larger residuals only for high-biomass tail samples, and Dry Clover shows the widest scatter, consistent with its 37.8% zero-inflation. Residuals are symmetric and centered near zero, confirming no systematic bias, and the tight Total scatter is encouraging given that compositional heads propagate component-level errors.

V. DISCUSSION

Implications for agricultural vision pipelines. Since global self attention is already performed across 24 transformer layers within each view by the DINOv3-ViT-L backbone, the fusion module need only enable local cross view communication, a role adequately served by kernel-5 depth-wise convolution. Global mechanisms (attention transformers, SSMS) introduce parameters that overfit on ~ 286 images per fold, a scale typical of precision agriculture datasets. A general design principle is thus indicated: fusion complexity should be matched to dataset scale, not task aspiration.

Cautionary lessons for metadata fusion in agriculture. A broader risk for agricultural pipelines that fuse heterogeneous

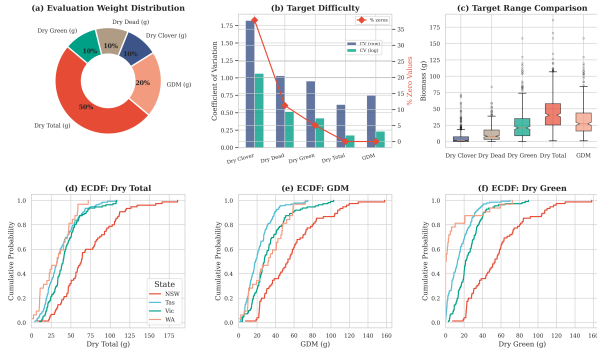


Fig. 13. Prediction quality analysis for the proposed model.

data sources is revealed by the metadata paradox: auxiliary features available only at training time can create harmful shortcuts. Predictive cues from species and state metadata (like “Lucerne in Victoria”) cause information to be routed through the metadata MLP at the expense of visual feature learning, and at test time, the strongest visual learner (GatedDWConv) suffers the largest degradation ($-7.4 R^2$ points). This finding is generalizable: any pipeline fusing training only auxiliary data (sensor readings, weather logs, field management records) risks the same shortcut, and modality dropout alone may be insufficient on small datasets.

Benchmarking position of CSIRO Biomass Dataset. Compared to GrassClover [33] (435 images, 2 Danish sites, May–October, no dead matter labels, and controlled lighting), CSIRO Biomass Dataset provides $2.7\times$ greater geographic diversity (19 sites, 4 states), year round coverage, dead matter annotations, camera diversity, and heterogeneous auxiliary inputs (NDVI, and height) absent from any comparable benchmark. Other agricultural vision datasets (CropHarvest, PlantNet, DeepWeeds, Agriculture-Vision) target classification, detection, or aerial segmentation, and none provides ground level, component wise biomass regression with laboratory validated measurements. CSIRO Biomass Dataset is thus the only appropriate benchmark for this study, and the 17 configuration suite serves as a reproducible reference for future work.

Limitations. All findings are derived from a single dataset, though no comparable alternative with laboratory validated, component wise biomass ground truth for proximal pasture imagery currently exists. The fusion complexity inversion may not hold with sufficient data, and the backbone comparison partially confounds pretraining data size with algorithmic improvements. At larger scales (like 2K–10K labeled images), complex global fusion modules would likely catch up to, or exceed local fusion. The 8GB VRAM limit constrains effective batch size and training throughput. Validation on emerging agricultural benchmarks with similar ground truth quality is left to future work.

VI. CONCLUSION

Foundation model adaptation for agricultural imagery is systematically studied on the 357 image CSIRO Pasture Biomass benchmark through 17 configurations. Three findings are established. First, *fusion complexity inversion*: a two layer gated depthwise convolution ($R^2=0.903$) outperforms cross view attention transformers (0.833), bidirectional SSMs (0.819), and full SSMs (0.793, below the no fusion baseline). Second, *foundation model dominance*: R^2 rises monotonically from EfficientNet-B3 (0.555) to DINOv3-ViT-L (0.903), confirming representation quality as the primary bottleneck. Third, *the metadata fusion trap*: training only metadata creates a ceiling at $R^2\approx 0.829$, collapsing an 8.4 point spread to 0.1 points. For scarce agricultural data, backbone quality should be prioritized, local fusion preferred, and inference-unavailable modalities excluded. Code: <https://github.com/WhiteMetagross/FusionComplexityInversionBiomass>

ACKNOWLEDGMENT

We gratefully acknowledge the Commonwealth Scientific and Industrial Research Organisation (CSIRO) for the creation, and public release of the CSIRO Pasture Biomass dataset, which made this research possible. Additionally, we disclose the use of AI assisted technologies: we utilized GPT 5.3 Codex, Claude Sonnet 4.6, and Claude Opus 4.6 for assistance with code implementation, grammar refinement, and writing and formatting support. Following the use of these tools, we thoroughly reviewed and edited the generated material as needed. We assume full responsibility for all scientific judgments, experimental design choices, and the final content of the manuscript.

REFERENCES

- [1] N. Jean, M. Burke, M. Xie, W. M. Davis, D. B. Lobell, and S. Ermon, “Combining satellite imagery and machine learning to predict poverty,” *Science*, vol. 353, no. 6301, pp. 790–794, 2016.
- [2] C. Adjorlolo, O. Mutanga, and M. A. Cho, “Estimation of canopy nitrogen concentration across C3 and C4 grasslands using WorldView-2 multispectral data,” *IEEE Journal of Selected Topics in Applied Earth Observations and Remote Sensing*, vol. 7, no. 11, pp. 4385–4392, 2014.
- [3] S. Bhojanapalli, W. Chen, A. Veit, and A. S. Rawat, “Understanding Robustness of Transformers for Image Classification,” in *Advances in Neural Information Processing Systems (NeurIPS)*, vol. 34, 2021.
- [4] M. Caron, H. Touvron, I. Misra, H. Jégou, J. Mairal, P. Bojanowski, and A. Joulin, “Emerging properties in self-supervised vision transformers,” in *Proceedings of the IEEE/CVF International Conference on Computer Vision (ICCV)*, pp. 9650–9660, 2021.
- [5] D. Wang, J. Zhang, B. Du, G. S. Xia, and D. Tao, “Self-supervised pre-training for remote sensing image analysis,” *IEEE Transactions on Geoscience and Remote Sensing*, vol. 60, pp. 1–16, 2022.
- [6] Y. Chen, X. Wang, Z. Zhang, and H. Liu, “Multi-view learning for fusion of multi-sensor data,” *Information Fusion*, vol. 79, pp. 75–94, 2022.
- [7] J. Ngiam, A. Khosla, M. Kim, J. Nam, H. Lee, and A. Y. Ng, “Multimodal deep learning,” in *Proceedings of the 28th International Conference on Machine Learning (ICML)*, pp. 689–696, 2011.
- [8] M. Rußwurm, N. Jacobs, and D. Tuia, “Meta-learning for cross-regional crop type mapping,” in *Proceedings of the IEEE/CVF Conference on Computer Vision and Pattern Recognition Workshops (CVPR Agriculture-Vision Workshop)*, 2023.
- [9] J. Gao, “NDVI – a review,” *Remote Sensing Reviews*, vol. 13, no. 1–2, pp. 145–174, 1996.
- [10] L. Petrich, G. Lohrmann, M. Neumann, and N. Weishaupt, “Estimation of ground cover and vegetation height from images using deep learning,” *Precision Agriculture*, vol. 21, no. 6, pp. 1243–1262, 2020.

- [11] S. A. Tsafaris, M. Minervini, and H. Schar, "Plant phenotyping with deep learning," *Annual Review of Plant Biology*, vol. 74, 2023.
- [12] A. Gu and T. Dao, "Mamba: Linear-time sequence modeling with selective state spaces," *arXiv preprint arXiv:2312.00752*, 2023.
- [13] I. Loshchilov and F. Hutter, "Decoupled weight decay regularization," in *International Conference on Learning Representations (ICLR)*, 2019.
- [14] P. Micikevicius, S. Narang, J. Alben, G. Diamos, E. Elsen, D. Garcia, B. Ginsburg, M. Houston, O. Kuchaiev, G. Venkatesh, and H. Wu, "Mixed precision training," in *International Conference on Learning Representations (ICLR)*, 2018.
- [15] Q. Liao, D. Wang, R. Haling, J. Liu, X. Li, M. Plomecka, A. Robson, M. Pringle, R. Pirie, M. Walker, and J. Whelan, "Estimating pasture biomass from top-view images: A dataset for precision agriculture," *arXiv preprint arXiv:2510.22916*, 2025.
- [16] Y. Liu, Y. Tian, Y. Zhao, H. Yu, L. Xie, Y. Wang, Q. Ye, J. Jiao, and Y. Liu, "VMamba: Visual state space model," *arXiv preprint arXiv:2401.10166*, 2024.
- [17] M. Oquab, T. Darcet, T. Moutakanni, H. Vo, M. Szafraniec, V. Khalidov, P. Fernandez, D. Haziza, F. Massa, A. El-Nouby, M. Assran, N. Ballas, W. Galuba, R. Howes, P. Y. Huang, S. W. Li, I. Misra, M. Rabbat, V. Sharma, G. Synnaeve, H. Xu, H. Jegou, J. Mairal, P. Labatut, A. Joulin, and P. Bojanowski, "DINOv2: Learning robust visual features without supervision," *Transactions on Machine Learning Research*, 2024.
- [18] O. Siméoni, H. V. Vo, M. Seitzer, F. Baldassarre, M. Oquab, C. Jose, V. Khalidov, M. Szafraniec, et al., "DINOv3," *arXiv preprint arXiv:2508.10104*, 2025.
- [19] A. Bauer, A. G. Bostrom, J. Ball, C. Applegate, T. Cheng, S. Laycock, S. M. Rojas, J. Kirwan, and J. Zhou, "Combining computer vision and interactive spatial statistics for the characterization of precision agriculture observations," *Computers and Electronics in Agriculture*, vol. 162, pp. 223–234, 2019.
- [20] D. Lu, "The potential and challenge of remote sensing-based biomass estimation," *International Journal of Remote Sensing*, vol. 27, no. 7, pp. 1297–1328, 2006.
- [21] C. F. Chen, Q. Fan, and R. Panda, "CrossViT: Cross-attention multi-scale vision transformer for image classification," in *Proceedings of the IEEE/CVF International Conference on Computer Vision (ICCV)*, pp. 357–366, 2021.
- [22] Y. H. H. Tsai, S. Bai, P. P. Liang, J. Z. Kolter, L. P. Morency, and R. Salakhutdinov, "Multimodal transformer for unaligned multimodal language sequences," in *Proceedings of the 57th Annual Meeting of the Association for Computational Linguistics (ACL)*, pp. 6558–6569, 2019.
- [23] L. Zhu, B. Liao, Q. Zhang, X. Wang, W. Liu, and X. Wang, "Vision Mamba: Efficient visual representation learning with bidirectional state space model," in *Proceedings of the 41st International Conference on Machine Learning (ICML)*, PMLR 235:62429–62442, 2024.
- [24] R. Xu, S. Yang, Y. Wang, Y. Cai, B. Du, and H. Chen, "A survey on vision mamba: Models, applications and challenges," *arXiv preprint arXiv:2404.18861*, 2024.
- [25] A. Hatamizadeh, H. Hosseini, N. Parchami, D. Terzopoulos, and J. Kautz, "MambaVision: A hybrid Mamba-Transformer vision backbone," *arXiv preprint arXiv:2407.08083*, 2024.
- [26] A. Dosovitskiy, L. Beyer, A. Kolesnikov, D. Weissenborn, X. Zhai, T. Unterthiner, M. Dehghani, M. Minderer, G. Heigold, S. Gelly, J. Uszkoreit, and N. Houlsby, "An image is worth 16x16 words: Transformers for image recognition at scale," in *International Conference on Learning Representations (ICLR)*, 2021.
- [27] A. Radford, J. W. Kim, C. Hallacy, A. Ramesh, G. Goh, S. Agarwal, G. Sastry, A. Askell, P. Mishkin, J. Clark, G. Krueger, and I. Sutskever, "Learning transferable visual models from natural language supervision," in *Proceedings of the 38th International Conference on Machine Learning (ICML)*, PMLR 139:8748–8763, 2021.
- [28] K. He, X. Chen, S. Xie, Y. Li, P. Dollár, and R. Girshick, "Masked autoencoders are scalable vision learners," in *Proceedings of the IEEE/CVF Conference on Computer Vision and Pattern Recognition (CVPR)*, pp. 16000–16009, 2022.
- [29] T. B. Brown, B. Mann, N. Ryder, M. Subbiah, J. Kaplan, P. Dhariwal, A. Neelakantan, P. Shyam, G. Sastry, A. Askell, S. Agarwal, A. Herbert-Voss, G. Krueger, T. Henighan, R. Child, A. Ramesh, D. M. Ziegler, J. Wu, C. Winter, C. Hesse, M. Chen, E. Sigler, M. Litwin, S. Gray, B. Chess, J. Clark, C. Berner, S. McCandlish, A. Radford, I. Sutskever, and D. Amodei, "Language models are few-shot learners," in *Advances in Neural Information Processing Systems (NeurIPS)*, vol. 33, pp. 1877–1901, 2020.
- [30] M. Tan and Q. V. Le, "EfficientNet: Rethinking model scaling for convolutional neural networks," in *Proceedings of the 36th International Conference on Machine Learning (ICML)*, PMLR 97:6105–6114, 2019.
- [31] A. Vaswani, N. Shazeer, N. Parmar, J. Uszkoreit, L. Jones, A. N. Gomez, L. Kaiser, and I. Polosukhin, "Attention is all you need," in *Advances in Neural Information Processing Systems (NeurIPS)*, vol. 30, pp. 5998–6008, 2017.
- [32] R. Wightman, "PyTorch image models (timm)," GitHub repository, <https://github.com/rwightman/pytorch-image-models>, 2019.
- [33] S. Skovsen, M. Dyrmann, A. K. Mortensen, K. A. Steen, O. Green, J. Eriksen, R. Gislum, R. N. Jørgensen, and H. Karstoft, "The Grass-Clover image dataset for semantic and hierarchical species understanding in agriculture," in *Proceedings of the IEEE/CVF Conference on Computer Vision and Pattern Recognition Workshops (CVPR Workshop)*, 2019.
- [34] E. Schulz, M. Speekenbrink, and A. Krause, "A tutorial on Gaussian process regression: Modelling, exploring, and exploiting functions," *Journal of Mathematical Psychology*, vol. 85, pp. 1–16, 2018.
- [35] D. Hendrycks and K. Gimpel, "Gaussian error linear units (GELUs)," *arXiv preprint arXiv:1606.08415*, 2016.
- [36] P. J. Huber, "Robust estimation of a location parameter," *The Annals of Mathematical Statistics*, vol. 35, no. 1, pp. 73–101, 1964.
- [37] Y. N. Dauphin, A. Fan, M. Auli, and D. Grangier, "Language modeling with gated convolutional networks," in *Proceedings of the 34th International Conference on Machine Learning (ICML)*, PMLR 70:933–941, 2017.
- [38] A. G. Howard, M. Zhu, B. Chen, D. Kalenichenko, W. Wang, T. Weyand, M. Andreetto, and H. Adam, "MobileNets: Efficient convolutional neural networks for mobile vision applications," *arXiv preprint arXiv:1704.04861*, 2017.
- [39] J. Deng, W. Dong, R. Socher, L. J. Li, K. Li, and L. Fei-Fei, "ImageNet: A large-scale hierarchical image database," in *Proceedings of the IEEE Conference on Computer Vision and Pattern Recognition (CVPR)*, pp. 248–255, 2009.
- [40] W. Guo, U. K. Rage, and S. Ninomiya, "Aerial imagery analysis – quantifying appearance and number of sorghum heads for breeding optimization," *Frontiers in Plant Science*, vol. 9, p. 1544, 2018.
- [41] N. Neverova, C. Wolf, G. Taylor, and F. Nebout, "ModDrop: Adaptive multi-modal gesture recognition," *IEEE Transactions on Pattern Analysis and Machine Intelligence*, vol. 38, no. 8, pp. 1692–1706, 2016.